encit 2022

ABCM Associação Brasileira de Engenharia e Ciências Mecânicas

19th Brazilian Congress of Thermal Sciences and Engineering
November 6th–10th, 2022, Bento Gonçalves - RS - Brazil

ENC-2022-0427
NUMERICAL INVESTIGATION OF THE HEAT TRANSFER OF A VISCOPLASTIC FLOW INSIDE A CAVITY WITH EMBEDDED CYLINDERS

Luiz Paulo Borges Miranda
Daniel Dall'Onder dos Santos
Federal University of Uberlândia, João Naves de Ávila Av., 2121, Uberlândia, MG, 38.408-100, Brazil
luiz.miranda@ufu.br, dallonder@ufu.br

Amir Roberto De Toni Jr.
Federal University of Rio Grande do Sul, Interdisciplinary Department, RS 030 km 92, 11700, Tramandaí, RS, 95590-000, Brazil
amir.detoni@ufrgs.br

Abstract. *A numerical study is performed to analyze the effects of Reynolds, plastic, and Richardson numbers on the non-isothermal, viscoplastic flow around two aligned cylinders embedded in a square enclosure under mixed convection conditions. The mechanical model is obtained by coupling the mass, momentum, and energy equations with the SMD viscoplastic model. The system of equations is solved using a Galerkin least-squares (GLS) type finite element method, and the average Nusselt number and displacement efficiency will be presented for each simulated case. The results point out that the heat transfer is generally enhanced by increasing the Richardson and Reynolds numbers; on the other hand, increasing the plastic number leads to an overall reduction in the average Nusselt number and a sudden drop in the displacement efficiency.*

Keywords: *viscoplastic flow, plastic number, mixed convection, SMD viscoplastic model, Galerkin least-squares method*

1. INTRODUCTION

The viscoplastic fluid behavior can be observed in a wide range of quotidian and engineering applications, in the form of foams, emulsions, and suspensions. Understanding of such phenomena involved in the fluid transport between reservoirs, containers, and through pipelines is increasing in importance due to the total added value of these products. In many applications the fluid is also being heated or cooled during the flow and, still, very little is known about the heat transfer characteristics of viscoplastic materials. Soares *et al.* (1999) numerically analyzed the heat transfer in the entrance region of tubes for Herschel-Bulkley fluid flows. The mechanical model was approximated via the finite volume method, and the authors also used constant wall heat flux and constant wall temperature to investigate the effects of temperature-dependent properties. Although not directly related to this work, since the viscosity function employed does not have a temperature dependency, general results showed significant differences in heat transfer if the fluid is simulated as temperature-dependent. Similar results were reported by Nouar *et al.* (1995), who carried out numerical analysis of the laminar forced convection in a cylindrical duct for a thermo-dependent Herschel-Bulkley fluid, also considering boundary conditions of constant wall heat flux and constant wall temperature. The governing equations were solved using the finite difference method assuming constant fluid properties except for the consistency index. The authors obtained correlations for the local Nusselt number and the pressure gradient considering the temperature-dependent characteristic of the fluid.

Laminar forced convection of viscoplastic fluids was also investigated by Nirmalkar *et al.* (2013), who studied the momentum and heat transfer characteristics of a heated square cylinder immersed in a streaming Bingham plastic medium. The mechanical model was numerically solved for a wide ranges of Reynolds, Prandtl, and Bingham numbers, and the authors reported that the unyielded regions expand with the increasing Bingham number, and due to the yield stress, the drag force on the cylinder is higher than that of a Newtonian fluid at the same Reynolds number. Numerical results obtained for the drag and Nusselt numbers were correlated to modified Bingham and Reynolds numbers via expressions enabling their interpolation for intermediate values of the governing parameters. More recently, Miranda *et al.* (2021) investigated the effects of Reynolds number, plastic number, and flow intensity $U^\star$ on the flow and the heat transfer of a viscoplastic SMD fluid flowing through a planar expansion followed by a contraction. The authors reported that the

Nusselt number has a positive dependence on the Reynolds number and flow intensity, as well as the increase in the fluid's displacement efficiency. On the other hand, the increase in the plastic number leads to a sudden decrease in the flow heat transfer and displacement efficiency. Severo *et al.* (2021) applied the Constructal Design Method to investigate how viscoplasticity affects the heat transfer on a row of circular tubes in crossflow configuration and to search for the best geometric shapes depending on the fluid rheology. The authors found a significant decrease in heat transfer with increasing yield stress limit and concluded that the optimum distance between cylinders, which maximized the heat transfer for fixed parameters except for the Bingham number, is always greater than those found in Newtonian flows. Similar investigations were performed by Shyam and Chhabra (2013) for tandem square cylinders immersed in power-law fluids and Tiwari and Chhabra (2015) for a semicircular cylinder immersed in Bingham fluids.

Regarding free convection in viscoplastic fluids, Sairamu *et al.* (2013) performed numerical simulations of Bingham fluids heat transfer from a heated horizontal circular cylinder in a square cavity. Using the finite-element based COMSOL solver, they evaluated the effects of different flow's dimensionless parameters and the ratio between cylinder diameter and square cavity size. Results showed that as the size of the cavity increases, both Bingham and average Nusselt numbers increase. A similar investigation was performed by Pandey *et al.* (2020) for a cylinder embedded in a square enclosure filled with power-law fluids. Free convection from a heated circular cylinder in Bingham fluid streams was investigated by Nirmalkar *et al.* (2014). The authors ranged the Rayleigh, Prandtl, and Bingham numbers, and observed a decrease in yielded regions with increasing Bingham number and with decreasing Rayleigh number, as the buoyancy-induced flow weakens.

Coupling the two convection heat transfer mechanisms, Srinivas *et al.* (2009) numerically studied the mixed convection heat transfer from a cylinder in power-law fluids and found that both drag coefficient and average Nusselt number increase with increasing buoyancy effects, Reynolds, and Prandtl numbers. Increases in the shear-thinning tendency of the fluid enhance both drag and heat transfer, whereas they are generally reduced in shear-thickening fluids. Additionally, buoyancy effects were stronger in shear-thinning fluids and at low Reynolds number regimes. Nalluri *et al.* (2015) and Bose *et al.* (2015) simulated the mixed heat transfer in Bingham fluids for a heated hemisphere and a heated cylinder, respectively. Both studies observed that increasing Reynolds or Prandtl numbers tend to enhance convection, and the yielded regions' size have a positive dependence on these parameters. On the other hand, increasing Bingham and Richardson numbers stabilizes the flow by suppressing the propensity of flow detachment. The average Nusselt number and drag coefficient show a positive dependence on the Richardson number, but this dependence progressively weakens with higher Bingham numbers. Santos (2016) performed numerical simulations of laminar flows over a cylinder immersed in viscoplastic SMD fluids subjected to mixed convection. The power-law index, Herschel-Bulkley, and Richardson numbers were varied to evaluate their influence on the cylinder heat transfer and drag coefficient. The increase of the Ri and HB numbers, as well as the increase in the n index, result in higher C_D. Regarding heat transfer, natural convection has a positive effect on the average Nusselt number, with the opposite behavior occurring when the power-law index increases, as the fluid becomes thicker and advection transport is reduced. The flow's viscoplastic level, measured by the HB number, delineates two different heat transfer behaviors. For $HB < 500$, due to the acceleration of the fluid near the cylinder surface, the Nusselt number is increased, while for $HB > 500$, even the cylinder vicinity is under strong viscoplastic effects – the flow is decelerated and the advection heat transport significantly decreases.

In this work, a finite element method is used to numerically solve the laminar mixed convection around two heated circular cylinders embedded in a square cavity subjected to a viscoplastic flow. Initially, the Newtonian fluid model is used to compare the employed methodology to the literature results. In a second step, the SMD fluid model is used to simulate the following range of conditions: Reynolds number from 10 to 100, the plastic number Pl from 0.1 to 0.9, and Richardson number from 0 to 1.

2. MECHANICAL MODEL

This work investigates the steady viscoplastic fluid flows around two heated cylinders embedded in a square cavity, as schematically shown in Fig. 1a. Natural-, forced- or even mixed-convection is present once the fluid enters the domain with a given temperature lower than the cylinders' surface temperature – the heat transfer regime depends on the prevailing flow conditions. To vary the fluid density with temperature, the Boussinesq approximation is used, given as $\rho = \rho_\infty[1 - \beta(T - T_\infty)]$, where β is the volumetric thermal expansion coefficient, T_∞ and ρ_∞ are the fluid temperature and density, respectively, imposed at the entrance of the flow domain.

The continuity, momentum balance, constitutive and energy equations, in a fixed Eulerian system, can be respectively

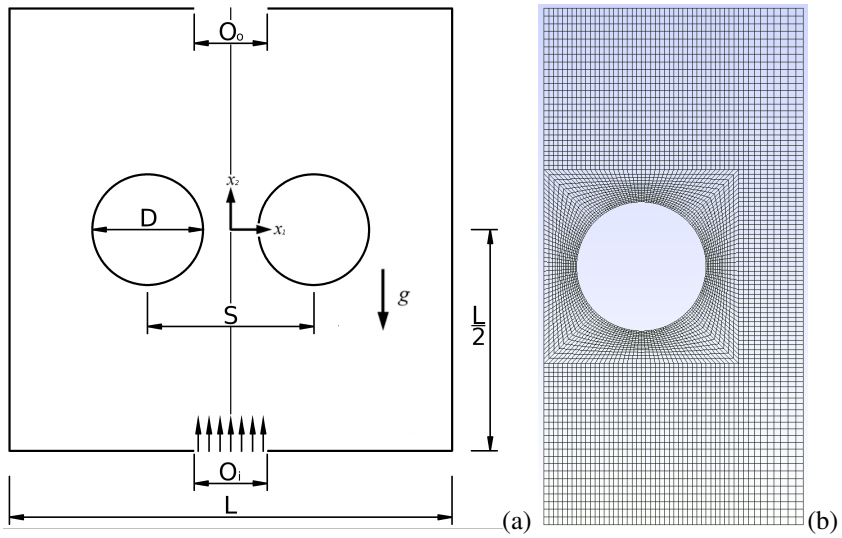

Figure 1. (a) Sketch of the geometry; (b) employed mesh.

expressed as

$$\begin{aligned}
&\rho_\infty \left(u_j \frac{\partial u_i}{\partial x_j} \right) = -\frac{\partial p}{\partial x_i} + \frac{\partial \tau_{ij}}{\partial x_j} + \rho_\infty g_i \beta (T - T_\infty), \\
&\frac{\partial u_i}{\partial x_i} = 0, \\
&\tau_{ij} = 2\eta(\dot{\gamma}) D_{ij}, \\
&\rho_\infty c_p \left(u_i \frac{\partial T}{\partial x_i} \right) = \kappa \left(\frac{\partial}{\partial x_i} \left(\frac{\partial T}{\partial x_i} \right) \right),
\end{aligned} \tag{1}$$

with

$$D_{ij} = \frac{1}{2} \left(\frac{\partial u_i}{\partial x_j} + \frac{\partial u_j}{\partial x_i} \right) \tag{2}$$

where u_i is the i component of the velocity vector, T is the temperature, p is the hydrostatic pressure, c_p and κ are the fluid specific heat and thermal conductivity, respectively; g_i is the i component of the gravity vector – in this work, the gravity vector is aligned with the negative direction of the x_2 axis, hence $g_1 = 0$; τ_{ij} and D_{ij} are the ij component of the extra-stress and strain rate tensors, respectively.

Some assumptions are made to ease the numerical solution: the specific heat and thermal conductivity are kept constant, and the viscosity does not depend on the temperature, only on the shear rate $\left(\dot{\gamma} = 2trD_{ij}{}^2)^{1/2}\right)$ according to the SMD viscosity model, proposed by de Souza Mendes and Dutra (2004) and modified by de Souza Mendes (2009). The modification avoids a non-physical behavior of the viscosity, which could tend to zero as the shear rate increases. The SMD model becomes

$$\eta(\dot{\gamma}) = \left(1 - \exp\left(-\frac{\eta_0}{\tau_0} \dot{\gamma} \right) \right) \left(\frac{\tau_0}{\dot{\gamma}} + K \dot{\gamma}^{n-1} \right) + \eta_\infty \tag{3}$$

where η_0 and η_∞ are, respectively, the viscosities for very low and very high values of the shear rate, τ_0 is the yield stress limit of the material, K is the consistency index, and n is the power-law index, which controls the shear-thinning and shear-thickening of the fluid when the material starts to flow.

2.1 Dimensionless groups of interest

In this work, the dimensionless groups of interest are: the Reynolds number (Re), the Richardson number (Ri), the plastic number (Pl), the Prandtl number (Pr), the jump number (J), and the Nusselt number (Nu). The adopted expressions for Re, Pr and Pl follow the definitions proposed by Thompson and Soares (2016):

$$Re = \frac{\rho {V_c}^2}{\tau_0 + K(\frac{V_c}{L_c})^n + \eta_\infty(\frac{V_c}{L_c})} \tag{4}$$

$$\frac{1}{Pr} = \frac{K(\frac{V_c}{L_c})^n + \eta_\infty(\frac{V_c}{L_c})}{\tau_0 + K(\frac{V_c}{L_c})^n + \eta_\infty(\frac{V_c}{L_c})} \frac{\rho\alpha}{K(\frac{V_c}{L_c})^{n-1} + \eta_\infty} \tag{5}$$

$$Pl = \frac{\tau_0}{\tau_0 + K(\frac{V_c}{L_c})^n + \eta_\infty(\frac{V_c}{L_c})} \tag{6}$$

where α is the thermal diffusivity, V_c and L_c are the characteristic velocity and characteristic length, respectively, taken as the average velocity at the inlet and the cylinder diameter (D).

The jump number (*J*) is a dimensionless group proposed by de Souza Mendes *et al.* (2007), and its expression is $J = (\eta_0\dot{\gamma}_1/\tau_0) - 1$ where $\dot{\gamma}_1 = (\tau_0/K)^{1/n}$. The dimensionless apparent viscosity and Ri number are defined as:

$$\eta^* = \frac{\eta}{\eta_0} \quad , \quad Ri = \frac{\mid \mathbf{g} \mid \beta\Delta T L_c}{U_c^2} \tag{7}$$

The displacement efficiency and the average Nusselt number are calculated as described by Miranda *et al.* (2021). The primal variables of the problem are expressed in a dimensionless form as:

$$x_i^* = \frac{x_i}{D} \ , \ u_i^* = \frac{u_i}{V_c} \ , \ \tau_{ij}^* = \frac{\tau_{ij}}{K}\left(\frac{D}{V_c}\right)^n \ , \ p^* = \frac{p}{\rho_\infty V_c^2} \ , \ T^* = \frac{T - T_\infty}{T_s - T_\infty} \ , \ \eta^* = \frac{\eta}{K}\left(\frac{D}{V_c}\right)^{n-1} \ , \ \dot{\gamma}^* = \dot{\gamma}\frac{D}{V_c} \tag{8}$$

where T_s is the cylinder surface temperature.

2.2 Geometry and boundary conditions

The fluid enters the cavity through an opening located at the bottom wall and exits at the top wall through an outlet with the same width ($O_i = O_o = 0.5D$). The distance between the centers of the cylinders (S) is $1.5D$. The ratio between cavity width L and D is equal to 4.

To reduce computational cost, only half of the geometry was simulated (Fig. 1b), with the symmetry line at x_1^*=0. The velocity boundary conditions were impermeability and no-slip on the cavity walls and cylinder surface, and a flat vertical velocity profile at the inlet, while at the symmetry line u_1 and τ_{12} were set equal to 0. The dimensionless temperature at the inlet was set to 0 and at the cylinder surface was set to 1, with the cavity walls and symmetry line being thermally insulated.

2.3 Numerical solution methodology

In this work, the numerical approximation of the mechanical model is done by employing the finite element method. A stabilized multi-field Galerkin least-squares formulation in terms of velocity, pressure and extra-stress is used to solve the fluid mechanical behavior (NNFEM routine) – see Zinani (2006), Zinani and Frey (2006), Zinani and Frey (2008), Frey *et al.* (2010) and Santos *et al.* (2011) for further details. This formulation, able to perform numerical simulations of non-Newtonian fluid flows, is a direct extension of the one introduced by Behr *et al.* (1993) for constant viscosity fluids. The thermal field is calculated using a separate routine (FEM90). For all calculations, equal-order bi-linear (Q1) finite element interpolations are used, and the solution is obtained using initial velocity and temperature guesses, e.g., an isothermal Newtonian flow. After the convergence of the two routines, the absolute error between two consecutive algorithm iterations for all the variables is evaluated. The result is stored and post-processed if the maximum error value is lower than 10^{-6} (Santos, 2016). The employed mesh contains 5540 bi-linear elements, resulting in 5768 nodal points (Fig. 1b), and was designed with a refinement at the cylinder vicinity, where the highest temperature and velocity gradients are found.

3. RESULTS

In this investigation, the influence of the Reynolds, Richardson and plastic numbers is evaluated, thus a default set of dimensionless numbers was chosen ($Pr = 1000$, $J = 1000$, $n = 0.5$, and $\eta^*_{\text{inf}} = 1 \times 10^{-8}$). For the mesh independence tests and comparison with the literature, the Newtonian viscosity model was employed. Results were obtained for $Re = 150$, $Pr = 0.7$, and $Ri = 0.1$ and 1, following the values employed by Ali and Alomar (2021). The thermal boundary conditions were altered for the cavity walls to allow an adequate comparison, since Ali and Alomar (2021) used a prescribed temperature condition ($T^* = 0$) instead of insulation.

3.1 Mesh independence tests and literature comparison

Three finite element discretizations were used for the mesh independence assessment: mesh 1 (M1), with 2770 elements; mesh 2 (M2), with 5540 elements; mesh 3 (M3), with 11080 elements. Although mesh M3 presented the lowest errors for the average Nusselt number when compared to the results of Ali and Alomar (2021) (Tab. 1), mesh M2 was selected to perform the simulations with viscoplastic fluid flows due to its reduced computational cost. Figure 2 shows the streamlines intensity and the dimensionless temperature fields, obtained for $Re = 150$, $Pr = 0.7$, and $Ri = 1$, by Ali and Alomar (2021) and the ones obtained in this work. Besides the favorable comparison for average Nusselt number, the present fields have also shown a good agreement.

Table 1. Average Nusselt number relative error between Ali and Alomar (2021) results and the three meshes employed in the present study.

	Mesh		
	M1	M2	M3
$Ri = 0.1$	5.13%	1.75%	1.21%
$Ri = 1$	4.45%	0.71%	0.52%

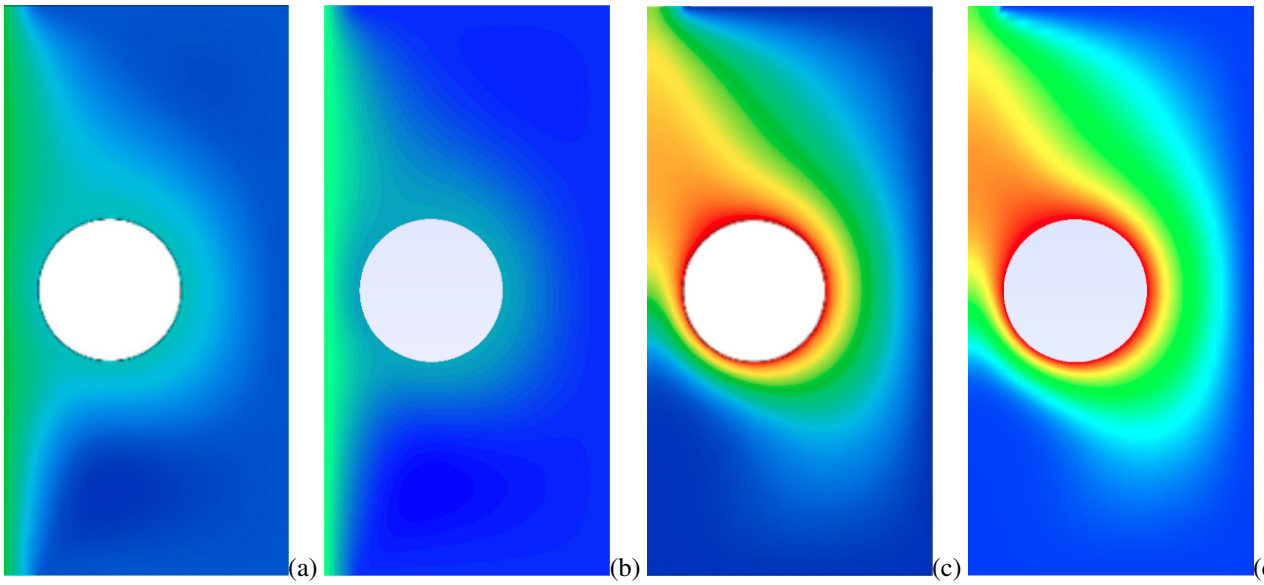

(a) (b) (c) (d)

Figure 2. Comparison with results from Ali and Alomar (2021), for $Re = 150$, $Pr = 0.7$, and $Ri = 1$: streamlines from (a) Ali and Alomar; (b) this work; dimensionless temperature from (c) Ali and Alomar, (d) this work.

3.2 Reynolds number variation

Figure 3a shows the effect of the Reynolds number on displacement efficiency for different plastic numbers. Due to the increasing inertial-to-viscous forces ratio, the fluid tends to flow directly from inlet to outlet, resulting in a decrease in displacement efficiency regardless of the plastic number. On the other hand, heat transfer from the cylinders' surfaces increases with the Reynolds number due to the same effect - the acceleration of the flow at the cavity's centerline and deceleration of the fluid at regions between cylinder and the vertical walls, as depicted in Fig. 4b at $x_2^* = 0$.

One can observe a similar behavior of the local Nusselt number at the left side of the cylinder in Fig. 4a for $Re = 50$ and 100. However, on the right side, the local Nusselt number has lower values, leading to a lower average Nusselt number (Fig. 3b). The same behavior was observed for $Pl = 0.1$ and 0.9, although the average Nusselt number presents a monotonic tendency for these values. This difference from the case with $Pl = 0.5$ is explained by a more pronounced reduction of the displacement efficiency, leading to fewer regions subjected to the fluid actually flowing around the cylinder. Fig. 5 shows the apparently unyielded regions (in black) for $Pl = 0.5$, $Ri = 0$, $Re = 10$ to 100, the criterion used being $\tau \leq \tau_0$.

3.3 Plastic number variation

Figure 6 shows the effects of the plastic number on the displacement efficiency and average Nusselt number for $Re = 10$, 50 and 100, keeping $Ri = 0$. Among the Reynolds numbers evaluated the behavior is quite similar, with a

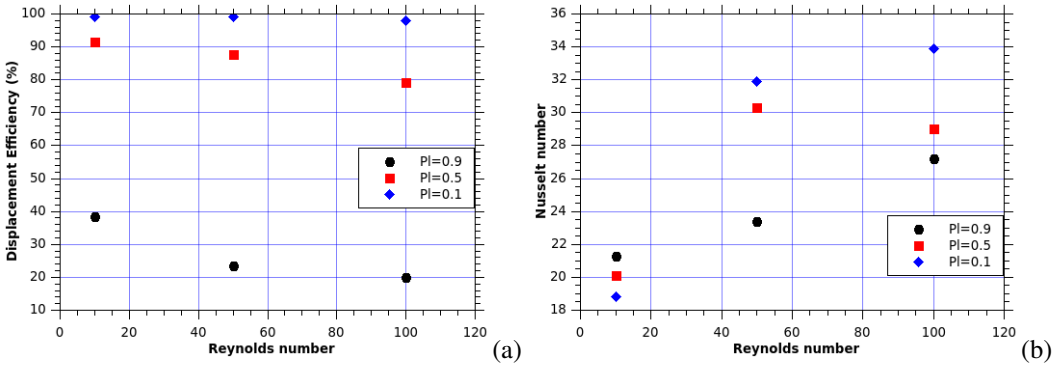

Figure 3. (a) Displacement efficiency and (b) average Nusselt number as a function of the Reynolds number, for $Ri = 0$.

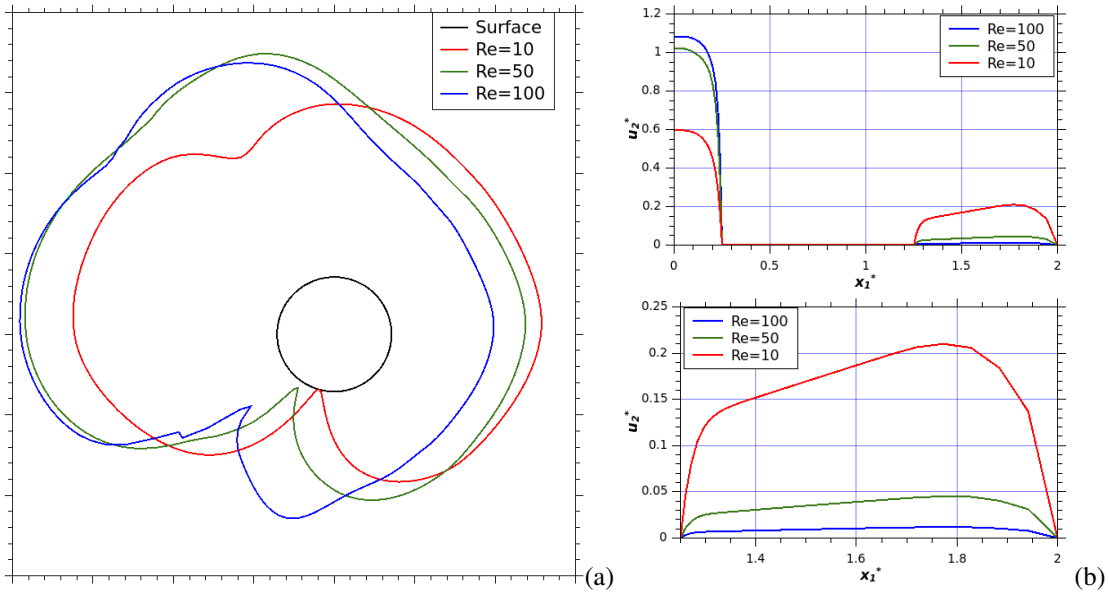

Figure 4. (a) Local Nusselt number distribution and (b) dimensionless vertical velocity profiles as a function of the Reynolds number, for $Pl = 0.5$ and $Ri = 0$, at $x_2^* = 0$.

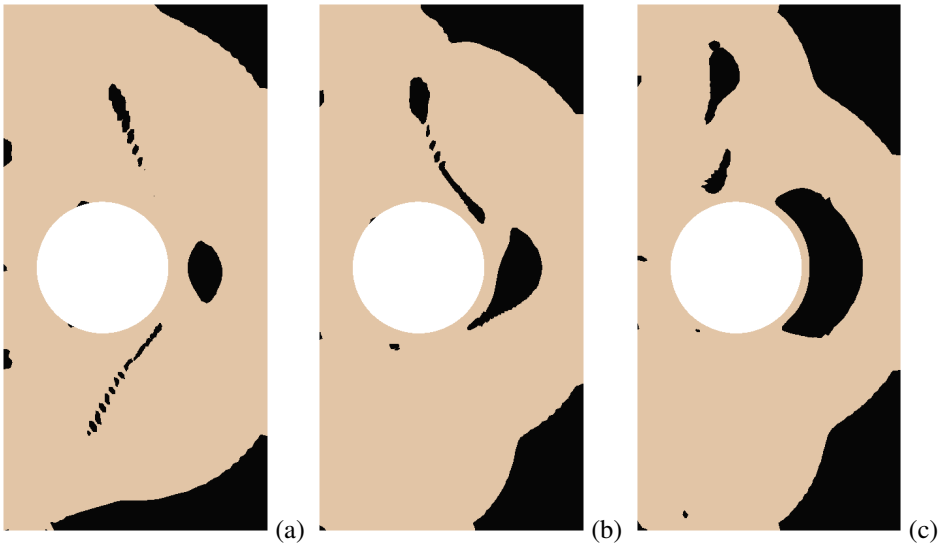

Figure 5. Apparently unyielded regions for $Pl = 0.5$, $Ri = 0$: (a) $Re = 10$; (b) $Re = 50$; (c) $Re = 100$.

significant drop in displacement efficiency as the flow's plasticity level is increased, with the unyielded regions shown on Fig. 8 for $Re = 10$ corroborating this conclusion.

Regarding heat transfer, two behaviors are noticeable. For $Re = 10$, the average Nusselt number increases with the plasticity level of the fluid. One plausible explanation for this behavior can be inferred from the velocity profiles on

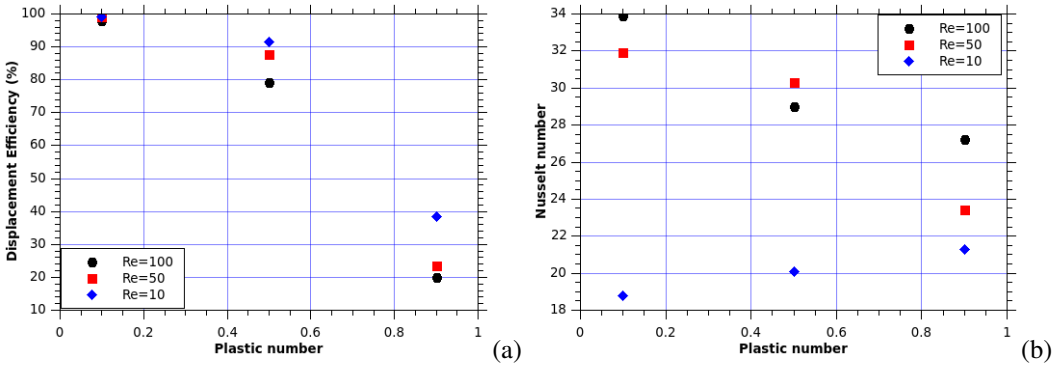

(a) (b)

Figure 6. (a) Displacement efficiency and (b) average Nusselt number as a function of the plastic number, for $Ri = 0$.

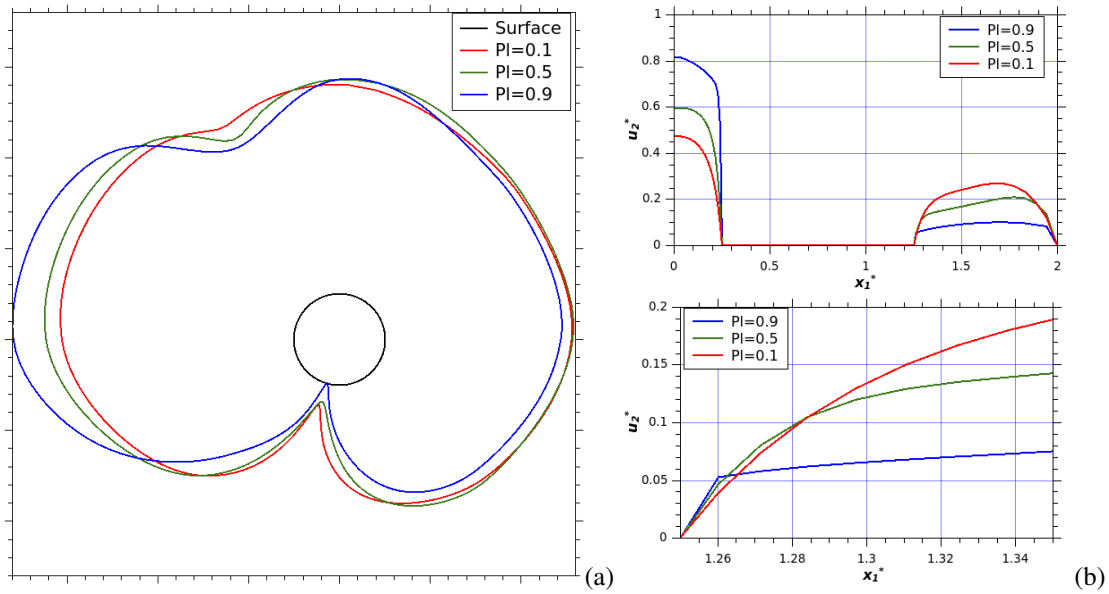

(a) (b)

Figure 7. (a) Local Nusselt number distribution and (b) dimensionless vertical velocity profiles as a function of the plastic number, for $Re = 10$ and $Ri = 0$, at $x_2^* = 0$.

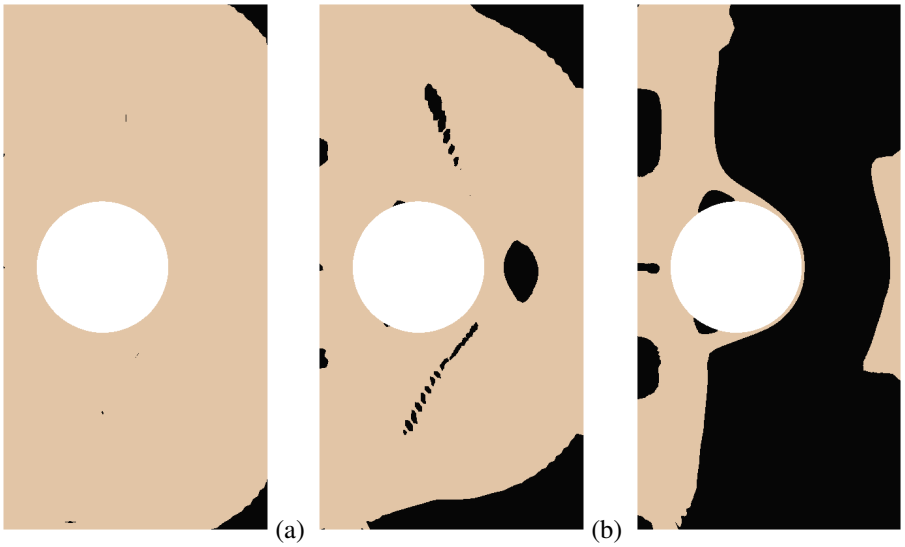

(a) (b) (c)

Figure 8. Apparently unyielded regions for $Re = 10$, $Ri = 0$: (a) $Pl = 0.1$; (b) $Pl = 0.5$; (c) $Pl = 0.9$.

the right-hand side of the cylinder surface. As depicted in the lower image in Fig. 7b, the case with the higher Pl has the highest vertical velocity near the surface at $x_2^* = 0$. As pointed out by Santos (2016), the fluid's acceleration and deceleration around the obstructing object is facilitated by the viscosity drop next to the solid surface. The other trend is

common for $Re = 50$ and 100, where the average Nusselt number drops with increasing flow plasticity. As the inertia effects are more intense, the core flow tends to go directly to the outlet, and local acceleration at the right-hand side of the cylinder is no longer observed - in fact, for $Re = 100$, the vertical velocity at this region is negative, indicating a very slow recirculation zone.

It is interesting to note the coincidence between the regions above the cylinder surface with lower local Nusselt numbers (see Fig. 7a) and the existence of an unyielded region attached to the surface (Fig. 8), besides the location of the flow stagnation point - where, for some cases, an unyielded region is also present.

3.4 Richardson number variation

The influence of the natural convection is shown in Figs. 9–11. Reasoning in terms of dimensionless quantities, the Richardson number is defined as $Ri = Gr/Re^2$, where Gr is the Grashof number, the ratio between the buoyancy and the viscous forces in the flow. Thus, an increase in the Richardson number represents a Gr increase, for a fixed Re. Since the gravity vector was considered aligned with the flow, though pointing in the opposite direction, the buoyancy effects add to the inertia effects. Considering the cases with $Re = 50$, the displacement efficiency is slightly affected by the increase in the Richardson number, with more pronounced effects observed for $Pl = 0.9$ (Fig. 9a). Figure 11 shows the unyielded zones of the flow for $Pl = 0.5$, and the main differences are located near the cylinder surface. On the other hand, the Nusselt number is positively affected by the increase of the mixed convection (Fig. 9b).

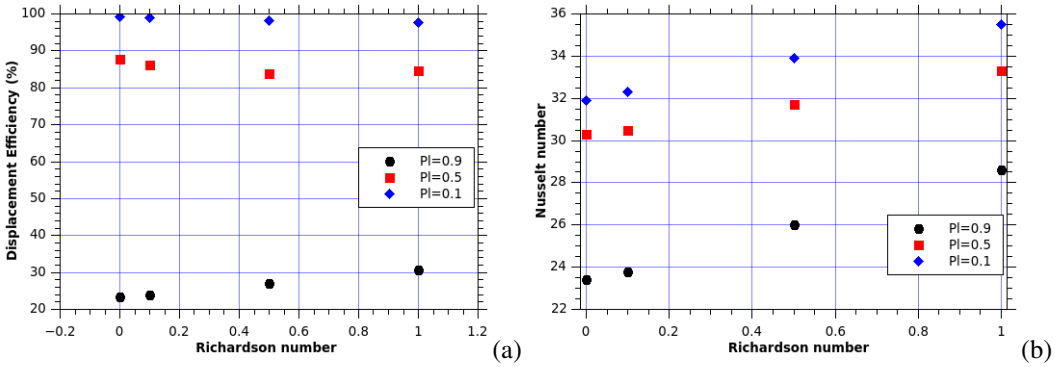

Figure 9. (a) Displacement efficiency and (b) average Nusselt number as a function of the Richardson number, for $Re = 50$.

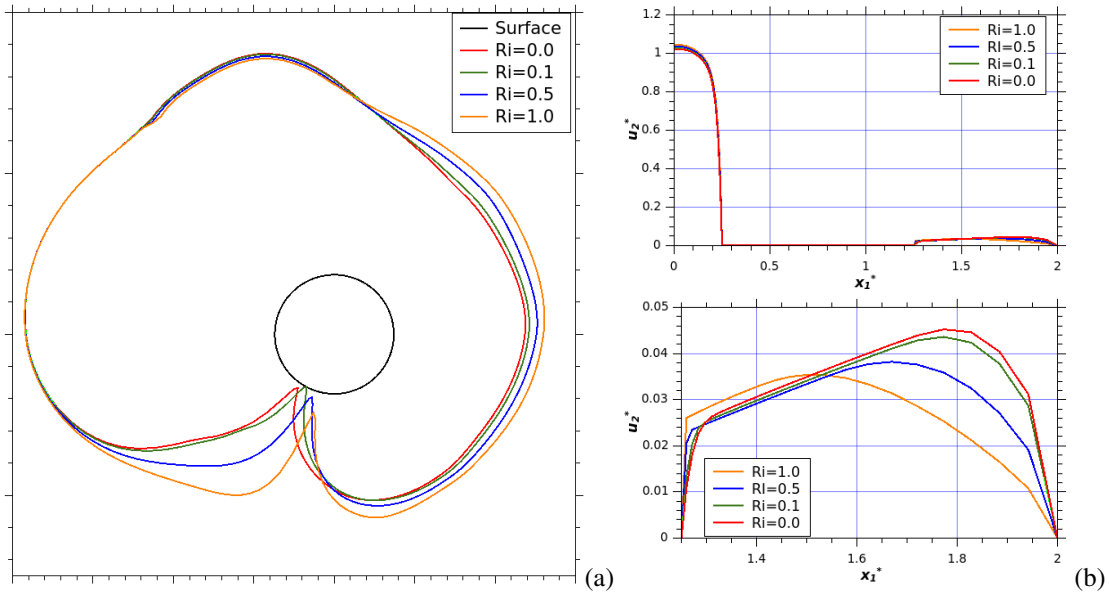

Figure 10. (a) Local Nusselt number distribution and (b) dimensionless vertical velocity profiles as a function of the plastic number, for $Re = 50$ and $Pl = 0.5$, at $x_2^* = 0$.

At a first glance, the effects on the velocity profile at $x_2^* = 0$ are not pronounced, but near the right-hand cylinder surface, the vertical velocity increases locally with Ri, which can be related to the increase in the displacement efficiency and the Nusselt number. The local Nusselt number distribution also demonstrates this effect, as well as the offset of the stagnation point slightly to the right.

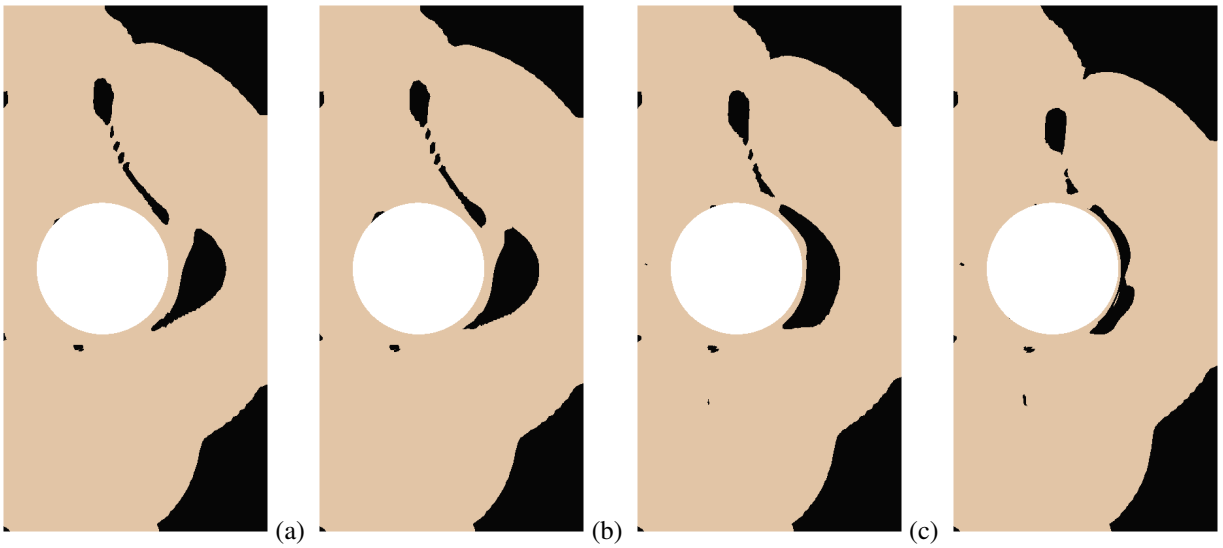

(a) (b) (c) (d)

Figure 11. Apparently unyielded regions for $Re = 50$, $Pl = 0.5$: (a) $Ri = 0$; (b) $Ri = 0.1$; (c) $Ri = 0.5$; (d) $Ri = 1.0$.

3.5 Summarized results

Tables 2 and 3 summarize the results obtained in this work. It is important to point out that the results for three conditions [$Re = 100$, $Ri = 0.5$, $Pl = 0.9$; $Re = 100$, $Ri = 1.0$, $Pl = 0.5$; and $Re = 100$, $Ri = 1.0, 0.9$] could not be obtained due to limitations in the numerical approximation. The aforementioned cases result in Rayleigh numbers ($Ra = Gr.Pr$) up to 5×10^6, meaning that turbulence effects need to be taken into account.

Table 2. Obtained results for the displacement efficiency (%).

	Re=10			*Re=50*			*Re=100*		
Ri	*Pl=0.1*	*Pl=0.5*	*Pl=0.9*	*Pl=0.1*	*Pl=0.5*	*Pl=0.9*	*Pl=0.1*	*Pl=0.5*	*Pl=0.9*
0	99.1	91.6	38.4	99.1	87.7	23.5	97.9	79.1	19.9
0.1	99.1	91.5	38.3	98.9	86.3	23.9	97.7	78.3	20.0
0.5	99.0	91.2	38.3	98.3	83.8	27.0	98.4	82.9	-
1	99	90.9	38.6	97.7	84.7	30.6	99.1	-	-

Table 3. Obtained results for the average Nusselt number.

	Re=10			*Re=50*			*Re=100*		
Ri	*Pl=0.1*	*Pl=0.5*	*Pl=0.9*	*Pl=0.1*	*Pl=0.5*	*Pl=0.9*	*Pl=0.1*	*Pl=0.5*	*Pl=0.9*
0	18.8	20.1	21.3	31.9	30.3	23.4	33.9	29.0	27.2
0.1	18.9	20.3	21.5	32.3	30.5	23.8	34.5	29.5	23.7
0.5	19.3	20.8	22.1	33.9	31.7	26.0	36.9	32.6	-
1	19.8	21.3	22.8	35.5	33.3	28.6	39.8	-	-

4. CONCLUDING REMARKS

This work presents a numerical study of non-Newtonian fluid flows inside a cavity with embedded cylinders. The flow dimensionless parameters, namely the Reynolds, plastic, and Richardson numbers were varied to evaluate the capability of heat exchange between the cylinders and the fluid and the effect on displacement efficiency. The Reynolds number has a positive effect on the heat transfer, but the displacement efficiency is hampered for higher plastic numbers. As mentioned, the plastic number has an overall negative influence on displacement efficiency and heat transfer. Natural convection positively affects the average Nusselt number and displacement efficiency, although its effect is small. It is also important to mention the stability of the solution methodology based on a finite element formulation, which provides satisfactory results even for coarse meshes, as is shown by the comparison with literature results.

5. ACKNOWLEDGMENTS

L.P.B. Miranda is grant holder of CNPq, process number 140729/2020-8. The authors acknowledge CAPES, FAPEMIG, and the Faculty of Mechanical Engineering (FEMEC/UFU) for financial support.

6. REFERENCES

Ali, O.M. and Alomar, O.R., 2021. "Mixed convection heat transfer from two aligned horizontal heated cylinders in a vented square enclosure". *Thermal Science and Engineering Progress*, Vol. 25, p. 101041. ISSN 2451-9049. doi: https://doi.org/10.1016/j.tsep.2021.101041.

Behr, A.M., Franca, L.P. and Tezduyar, T.E., 1993. "Stabilized finite element methods for the velocity – pressure – stress formulation of incompressible flows". *Computer Methods in Applied Mechanics and Engineering*, Vol. 104, pp. 31–48.

Bose, A., Nirlmalkar, N. and Chhabra, R.P., 2015. "Effect of aiding-buoyancy on mixed-convection from a heated cylinder in Bingham plastic fluids". *Journal of Non-Newtonian Fluid Mechanics*, Vol. 220, pp. 3–21.

de Souza Mendes, P.R., 2009. "Modeling the thixotropic behavior of structured fluids". *Journal of Non-Newtonian Fluid Mechanics*, Vol. 164, pp. 66–75.

de Souza Mendes, P.R. and Dutra, E.S.S., 2004. "Viscosity function for yield-stress liquids". *Applied Rheology*, Vol. 14, pp. 296–302.

de Souza Mendes, P.R., Naccache, M.F., Varges, P.R. and Marchesini, F.H., 2007. "Flow of viscoplastic liquids through axisymmetric expansions-contractions". *Journal of Non-Newtonian Fluid Mechanics*, Vol. 142, pp. 207–217.

Frey, S.L., Silveira, F.S. and Zinani, F.S.F., 2010. "Stabilized mixed approximations for inertial viscoplastic fluid flows". *Mechanics Research Communications*, Vol. 37, pp. 145–152.

Miranda, L.P.B., dos Santos, D.D. and Zinani, F.S.F., 2021. "Effects of reynolds number, plastic number, and flow intensity on the flow and on the heat transfer of a viscoplastic fluid flowing through a planar expansion followed by a contraction". *International Communications in Heat and Mass Transfer*, Vol. 120, p. 105038. ISSN 0735-1933. doi:https://doi.org/10.1016/j.icheatmasstransfer.2020.105038.

Nalluri, S.V., Patel, S.A. and Chhabra, R., 2015. "Mixed convection from a hemisphere in bingham plastic fluids". *International Journal of Heat and Mass Transfer*, Vol. 84, pp. 304–318.

Nirmalkar, N., Bose, A. and Chhabra, R.P., 2014. "Free convection from a heated circular cylinder in bingham plastic fluids". *International Journal of Thermal Sciences*, Vol. 83, pp. 33–44.

Nirmalkar, N., Chhabra, R.P. and Poole, R.J., 2013. "Laminar forced convection heat transfer from a heated square cylinder in a bingham plastic fluid". *International Journal of Heat and Mass Transfer*, Vol. 56, pp. 625–639.

Nouar, C., Lebouché, M., Devienne and Riou, C., 1995. "Numerical analysis of the thermal convection for herschel-bulkley fluids". *International Journal of Heat and Fluid Flow*, Vol. 13, pp. 223–232.

Pandey, S., Park, Y.G. and Ha, M.Y., 2020. "Unsteady analysis of natural convection in a square enclosure filled with non-newtonian fluid containing an internal cylinder". *Numerical Heat Transfer, Part B: Fundamentals*, Vol. 77, No. 1, pp. 1–21. doi:10.1080/10407790.2019.1685838.

Sairamu, M., Nirmalkar, N. and Chhabra, R., 2013. "Natural convection from a circular cylinder in confined bingham plastic fluids". *International Journal of Heat and Mass Transfer*, Vol. 60, pp. 567–581.

Santos, D.D., 2016. "Numerical simulation of mixed convection from a cylinder immersed in viscoplastic fluids". In *Proceedings of the 16th Brazilian Congress of Thermal Sciences and Engineering - ENCIT 2016*. Vitória, Brazil.

Santos, D.D., Frey, S.L., Naccache, M.F. and de Souza Mendes, P.R., 2011. "Numerical approximations for flow of viscoplastic fluids in a lid-driven cavity". *Journal of Non-Newtonian Fluid Mechanics*, Vol. 166, pp. 667–679.

Severo, L.F., Zinani, F.S.F. and Rocha, L.A.O., 2021. "Constructal design analysis of viscoplastic cross-flow over a row of cylinders". *International Communications in Heat and Mass Transfer*, Vol. 122, p. 105147. ISSN 0735-1933. doi:https://doi.org/10.1016/j.icheatmasstransfer.2021.105147.

Shyam, R. and Chhabra, R.P., 2013. "Effect of prandtl number on heat transfer from tandem square cylinders immersed in power-law fluids in the low reynolds number regime". *International Journal of Heat and Mass Transfer*, Vol. 57, pp. 742–755.

Soares, M., Naccache, M.F. and de Souza Mendes, P.R., 1999. "Heat transfer to viscoplastic materials flowing laminarly in the entrance region of tubes". *International Journal of Heat and Fluid Flow*, Vol. 20, pp. 60–67.

Srinivas, A.T., Bharti, R.P. and Chhabra, R.P., 2009. "Mixed convection heat transfer from a cylinder in power-law fluids: effect of aiding buoyancy". *Industrial & Engineering Chemistry Research*, Vol. 48, pp. 9735–9754.

Thompson, R.L. and Soares, E.J., 2016. "Viscoplastic dimensionless numbers". *Journal of Non-Newtonian Fluid Mechanics*, Vol. 238, pp. 57–64.

Tiwari, A.K. and Chhabra, R.P., 2015. "Momentum and heat transfer from a semi-circular cylinder in bingham plastic fluids". *Applied Mathematical Modelling*, Vol. 39, pp. 7045–7064.

Zinani, F.S.F., 2006. *Desenvolvimento e Implementação Computacional de Formulações Galerkin Mínimos-Quadrados*

para Escoamentos Não-Newtonianos Sensíveis à Cinemática. Ph.D. thesis, Programa de Pós Graduação em Engenharia Mecânica da Universidade Federal do Rio Grande do Sul – UFRGS.

Zinani, F.S.F. and Frey, S.L., 2006. "Galerkin least-squares finite element approximations for isochoric flows of viscoplastic liquids". *Journal of Fluids Engineering*, Vol. 128, No. 4, pp. 856–863.

Zinani, F.S.F. and Frey, S.L., 2008. "Galerkin least-squares multifield approximations for flows of inelastic non-newtonian fluids". *Journal of Fluids Engineering*, Vol. 130, pp. 1–14.

7. RESPONSIBILITY NOTICE

The authors are solely responsible for the printed material included in this paper.